Swansea University
Prifysgol Abertawe

Cronfa
Setting Research Free

Cronfa - Swansea University Open Access Repository

_____

This is an author produced version of a paper published in :
Nanotechnology

Cronfa URL for this paper:
http://cronfa.swan.ac.uk/Record/cronfa22080

_____

Paper:

_____

UV photodecomposition of zinc acetate for the growth of ZnO nanowires

J S Lloyd[1], C M Fung[1], E J Alvim[1], D Deganello[2], K S Teng[1*]

[1] Multidisciplinary Nanotechnology Centre, College of Engineering, Swansea University, Singleton Park, Swansea SA2 8PP, UK

[2] Welsh Centre for Printing and Coating, College of Engineering, Swansea University, Singleton Park, Swansea SA2 8PP, UK

* Corresponding Author: K.S.Teng@Swansea.ac.uk

Abstract

The thermal annealing of zinc precursors to form suitable seed layers for the growth of ZnO nanowires is common. However, the process is relatively long and involves high temperatures which limit substrate choice. In this study the use of a low temperature, ultra-violet (UV) exposure is demonstrated for photodecomposition of zinc acetate precursors to form suitable seed layers. Comparisons are made between ZnO nanowire growth performed on seed layers produced through thermal annealing and exposure to UV. The dependence of growth density and nanowire diameter on UV exposure time is investigated. Growth quality is confirmed with energy dispersive x-ray (EDX) and x-ray diffraction (XRD) analyses. The chemical composition of the exposed layers is investigated with EDX and X-ray photoelectron spectroscopy (XPS). Atomic force microscopy (AFM) is utilized to investigate morphological changes with respect to UV exposure. The diameter and density of the resultant growth was found to be strongly dependent on the UV exposure time. UV exposure times of only 25 to 30 seconds led to maximum density of growth and minimum diameter, significantly faster than thermal annealing. EDX, XPS and AFM analyses of the seed layers confirmed decomposition of the zinc precursor and morphological changes which influenced the growth.

1. Introduction

Zinc oxide (ZnO) nanostructures have attracted much research and commercial interest due to their many unique properties, such as direct wide band gap (3.37 eV), high anisotropic configurations, piezoelectric characteristics and biocompatibility. Large surface to volume ratios of such nanostructures enable ultra-high sensitivity sensing. Furthermore, ZnO nanowires possess specific electronic and optical properties which stem from the high binding energy of 60 meV. Hence the properties of ZnO nanostructures has led to many potential applications, such as light emitting diodes (Ahn *et al* 2011), UV lasers (Huang *et al* 2001), UV detectors (Yi *et al* 2014), photo-voltaic devices (Guerguerian *et al* 2011, Hsueh *et al* 2012), gas sensors (Tarat *et al* 2012, Wang *et al* 2012, Lim *et al* 2011), chemical sensors and biosensors (Ali *et al* 2011, Yang *et al* 2009).

For ZnO nanowires to be utilized as part of a device they must be grown, generally directly onto the surface of these devices, during fabrication. The growth of ZnO nanowires can be categorized into vapour-phase and hydrothermal techniques. Vapour-phase synthesis of ZnO nanowires produces high quality structures with low density of defects. However, vapour phase synthesis, such as chemical vapour deposition (CVD) (Ok *et al* 2010, Smith *et al* 2015), vapour-solid (VS) (Wang 2004, Yoon *et al* 2008), vapour-liquid-solid (VLS) (Zacharias *et al* 2010, Fan *et al* 2006), and thermal evaporation (Kar *et al* 2006), require high process temperatures (700°C to 900°C), high cost equipment setups and also involve complex and difficult process control. For these reasons, vapour phase synthesis lacks suitability for low cost volume production. The high process temperatures also limit the substrate types, onto which these devices can be fabricated, again influencing the cost and diversity of devices which can utilize such nanostructures. However, the development of aqueous hydrothermal techniques (Greene *et al* 2003, Akgun *et al* 2012, Baruah and Dutta 2009b) opens the possibility of mass production due to the low temperatures of less than 100°C, low setup costs and simplified process control. This low temperature also allows the flexibility of being able to choose from a much wider range of substrates, such as polymers. For this reason the hydrothermal growth of ZnO nanowires is favourable in device fabrication.

The hydrothermal growth of ZnO nanowires, directly onto a substrate, requires a seed layer to nucleate the growth. This layer must be uniform and for many applications must also be selectively patterned to enable growth in specific areas of the sample. The quality of the seed layer is important because the seed layer plays a vital role in the morphology of the resultant growth (Song and Lim 2007). Several methods exist for the formation of a suitable seed layer such as sputter deposition (Song and Lim 2007, Yang *et al* 2014) and zinc acetate derived seed layers (Bai 2011, Greene *et al* 2005, Gowthaman *et al* 2011, Hong *et al* 2013). Methods such as sputter deposition tend to yield highly uniform seed layers and also have the benefit of being able to accurately pattern the seed layer through photolithography. These processes, however, are high cost due to the use of expensive

equipment, they can also be limiting on the type of substrate available for use as the chemicals used in the photolithography process can be damaging to many polymer substrates. The use of zinc acetate solutions for the formation of seed layers provides a popular alternative. Although these solutions take many forms and a variety of deposition methods exist, the active reagent is the zinc acetate. The disadvantage, however, is the annealing process that is required for the thermal decomposition of the zinc acetate to form ZnO nanocrystallites, which become the seed layer. Generally, this annealing process is carried out on a hot plate or in an oven for a period of between 10 minutes (Hosono *et al* 2004) and 5 hours (Baruah and Dutta 2009a) at elevated temperatures of between 150°C (Wahid *et al* 2013) and 350°C (Plakhova *et al* 2012). This process is long and requires relatively high temperatures which limit the use of polymer substrates. The thermal decomposition of zinc acetate by local heating through the use of a laser has been explored by Hong et al (Hong *et al* 2013). However, this technique requires a gold layer and may limit the use of organic substrates due to heating.

To address this problem, enabling a wider range of substrate materials while reducing the annealing time and temperature, the work presented here investigates a faster, low temperature method for creating suitable seed layers for ZnO nanowire growth. The use of UV exposure to cause photodecomposition of the zinc acetate layer to form a suitable seed layer is demonstrated. This process could be incorporated into a printing process like flexographic printing. Flexographic printing has been investigated previously by the authors for the deposition of inks containing zinc acetate for the purpose of creating a seed layer suitable for the growth of ZnO nanowires (Lloyd *et al* 2013). Others have also investigated alternative printing methods such as inkjet for the same purpose (Liang *et al* 2013, 2009, Kwon *et al* 2013, Kitsomboonloha *et al* 2009). With the roll to roll nature of the flexographic printing technique and the use of low cost polymer substrates, devices could be mass produced with a high throughput at relatively low cost. Therefore, the development of a fast annealing process such as UV exposure investigated here is of technological importance.

The UV decomposition of zinc acetate for the production of seed layers has been demonstrated here on printed conductive electrodes on polymer substrates suitable for low cost fabrication. The process led to high quality, dense and uniform growth of ZnO nanowires. The effect of UV exposure time on the resultant ZnO nanowire growth was investigated along with compositional and morphological changes in the seed layer due to UV exposure. It is shown that significantly less time is required to form a suitable seed layer when using UV exposure as compared to thermal annealing. Furthermore, the significantly reduced ambient temperature allows a wider range of low cost plastic substrates to be used in the fabrication of devices incorporating ZnO nanowires.

2. Methods

2.1. Materials

The ink solutions consist of isopropanol (IPA) (Fisher scientific), zinc acetate dihydrate (Sigma Aldrich) and deionized water. Zinc acetate dihydrate and hexamethylenetetramine (HMTA) were required for the hydrothermal growth of the ZnO nanowires, these were purchased from Sigma Aldrich. The Carbon electrodes were printed with carbon flexographic ink 32% solids (Gwent electronic materials Ltd, C2080529P7) onto Cirlex Polyimide sheet of 0.15 mm thickness purchased from Lohmann Technologies UK Ltd. All chemicals used were of analytical grade and used without further purification.

2.2. Sample preparation

Samples were prepared by printing a layer of conductive carbon ink onto the surface of a polyimide substrate using an IGT Reprotest Printability Tester F1 Flexographic printer. The ink was then dried at 150°C for 10 minutes. Following this the zinc acetate precursor ink was prepared as previously described (Lloyd *et al* 2013). The ink consisted of 20% water, 80% IPA and contained a concentration of 0.1 M zinc acetate dihydrate. This solution was then simply drop cast onto the prepared printed carbon electrode on polyimide or onto bare silicon substrates. Carbon printed polyimide substrate was used to demonstrate the suitability of UV photodecomposition technique for scaled up production of ZnO nanowire devices. Silicon substrates were used to allow better characterization of the seed layer due to its higher conductivity and chemical purity.

After drop casting the zinc acetate precursor ink onto the samples, they were placed into the UV curing machine (Novascan, PSD Pro digital UV ozone system, with a UV lamp generating UV light at both 185 nm and 254 nm) for a duration of 5 seconds up to 120 seconds. After exposure, the samples were analysed to confirm the decomposition of zinc acetate with respect to the UV exposure time. Comparative control samples were annealed on a hot plate and in an oven at 150°C without UV exposure.

2.3. Growth

After the preparation of seeded samples, hydrothermal growth was performed. This allowed the study of the seed layer quality by assessing the resultant growth on the samples. The growth procedure, adapted from Akgun *et al* (Akgun *et al* 2012), was performed at 70°C in 200 ml of growth solution. The growth solution consisted of 10 mM zinc acetate dihydrate and 10 mM HMTA, mixed at room temperature. The growth solution was then placed in a preheated water bath at 70°C for 30 minutes. The sample was dipped in preheated (70°C) deionized water for 5 seconds prior to floating the sample on the surface of the growth solution. The sample was then left for 6 hours to grow ZnO nanowires. It was found that the preheating of the sample prior to growth reduced the formation of a nonselective

seeding layer, formed when a cold sample enters hot growth solution. Once the samples were removed from the growth solution they were vigorously washed with deionised water to remove any growth solution from the surface.

2.4. Characterization

The quality of the resultant ZnO nanowire growth was studied with a Hitachi S-4800 scanning electron microscope (SEM) at 10 kV to obtain topographical information such as diameter, shape and density of growth. The SEM was equipped with an Oxford Instruments energy-dispersive x-ray detector (EDX) employed to determine the elemental composition of the grown samples. The EDX was also used to assess changes in the elemental composition of the seed layers with respect to UV exposure time. A Bruker D8 Discover x-ray diffraction (XRD) system, equipped with a Cu_Kα x-ray source and a Lynxeye detector, was employed to evaluate the crystallinity of the as grown ZnO nanowires. Furthermore x-ray photoelectron spectroscopy (XPS) was used to evaluate the structure and composition of the seed layers with respect to UV exposure. The XPS experiments were carried out at room temperature using the Kratos Axis Supra system equipped with a monochromatic Al Kα source having an energy of 1486.6 eV. To investigate surface morphology of the seed layers a JPK Instruments atomic force microscope (AFM) was used in AC mode using tapping mode RTESP AFM probes (Bruker, USA). Images were subsequently analysed using scanning probe image processor (SPIP) image analysis software.

3. Results and Discussion

UV exposed samples were compared with control samples, such as non-annealed and thermally annealed samples. For non-annealed samples the ink was simply air dried. Annealed control samples were produced by introducing common thermal annealing processes, as described below.

Topographical SEM images of resultant ZnO nanowire growth performed on four different types of control samples are shown in figure 1. These samples were prepared as follows, (a) a seed layer which was not annealed, (b) a seed layer which was annealed on a hot plate at 150°C for 30 minutes, (c) a seed layer which was annealed in an oven at 150°C for 10 minutes and (d) a seed layer which was annealed in an oven at 150°C for 30 minutes. Non-annealed samples showed very little growth. In some small areas where growth was found as shown in figure 1(a), it was sparse and consisted of large wires typically greater than 350 nm in diameter. The thermally annealed control samples showed, as predicted, dense growth of much thinner nanowires. However, the hotplate annealed seed layer tended to result in more irregular growth directions and large variations in nanowire diameters. The oven annealed samples showed an improvement in density and uniformity. Further improvement was seen for growth on seed layers annealed for 30 minutes duration as compared to 10 minutes.

Samples annealed in the oven for 30 minutes produced nanowires of approximately 25 nm in diameter.
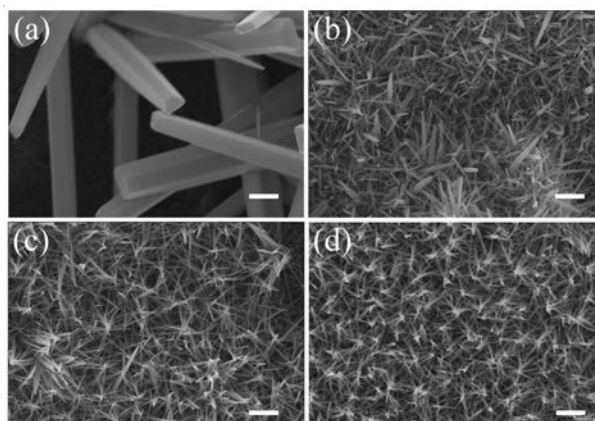

Figure 1: SEM images of ZnO nanowire growth on control samples (a) non-annealed seed layer, (b) hotplate annealed seed layer (30 minutes), (c) oven annealed seed layer (10 minutes) and (d) oven annealed seed layer (30 minutes). Scale bars indicate 500 nm.

For the UV exposure process, samples were exposed to UV for different durations. This was to establish how much UV exposure was required to cause sufficient decomposition of the zinc acetate to achieve a suitable seed layer for the ZnO nanowire growth. Samples were annealed for 5, 15, 25, 30, 45, 60 and 120 seconds, significantly less time than that of thermal annealing. SEM images of the resultant growth are shown in figure 2 and they show an interesting trend in the nanowire diameter and density of growth. After only 5 seconds of exposure the growth density is significantly greater than that of the non-annealed control sample. As the exposure time is increased, the density of nanowires increases and the diameter decreases. Beyond 25 to 30 seconds the density of growth begins to decrease again and the diameter of the nanowires begins to increase. This is shown graphically in figure 3 which clearly shows the trends in the density of growth and diameter of the nanowires versus UV exposure time. A clear trend can be seen on this graph showing the increase in nanowire density with increased exposure time, up to 30 seconds where the nanowire density then decreases as the exposure time further increases. It can also be seen that the trend in the diameter of the nanowires is the inverse of the growth density.
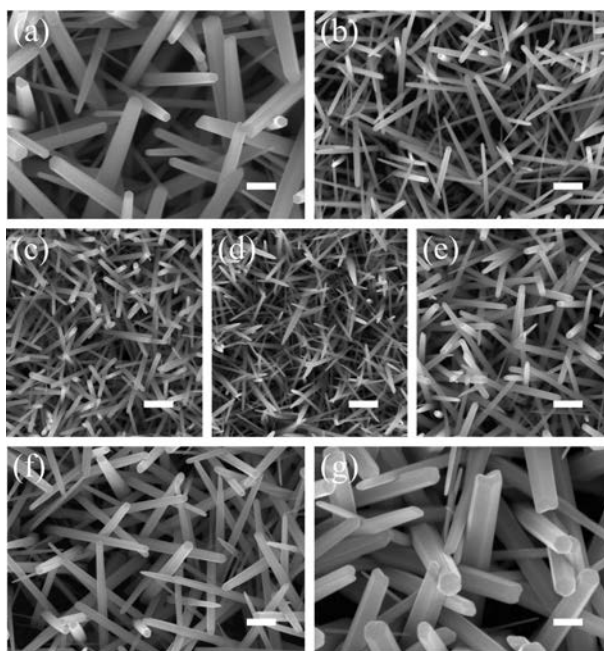
Figure 2: SEM images of UV annealed seed layers after ZnO nanowire growth with varying exposure times of (a) 5 s, (b) 15 s, (c) 25 s, (d) 30 s, (e) 45 s, (f) 60 s and (g) 120 s. Scale bar indicates 500 nm.
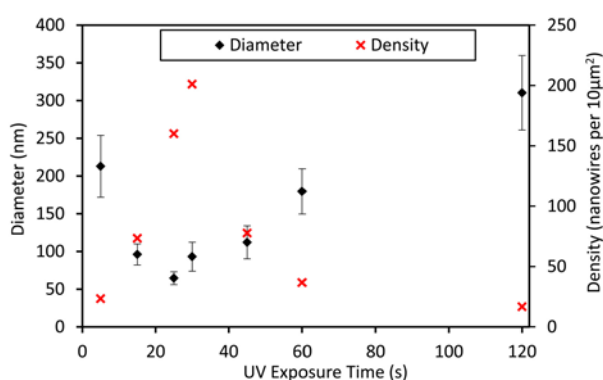

Figure 3: Graph of ZnO nanowire diameter (diamonds) and density (crosses) after growth vs. UV exposure time.

EDX and XRD analyses on the resultant growth show that the nanowires were of ZnO with high crystallinity. Figure 4 shows the EDX spectrum taken from a sample grown on a seed layer after 25 seconds of UV exposure time. The result confirms the chemical purity of the sample with only carbon, oxygen and zinc present in the spectra. The carbon contribution is due to the underlying carbon printed polyimide substrate and the zinc and oxygen are from the ZnO nanowires. Compositional analysis of the spectra revealed the zinc to oxygen ratio to be almost 1, demonstrating the typical 1:1 stoichiometry of ZnO. This result was typical of all of the samples from 5 to 120 seconds of UV exposure.
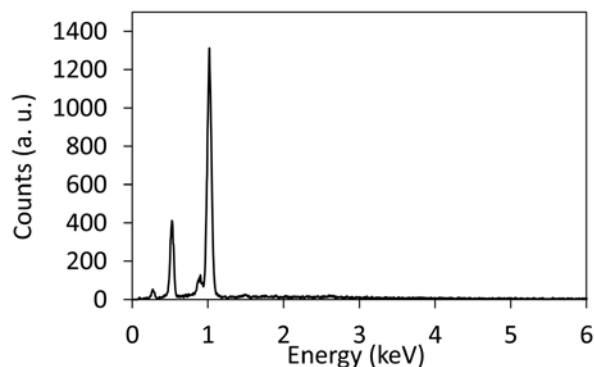
Figure 4: EDX analysis of ZnO nanowires grown on a seed layer after 25 seconds UV exposure time.

Figure 5 shows XRD analysis for growth on a seed layer which was exposed for 25 seconds and represents a typical result for exposure times between 5 and 120 seconds. XRD analysis of the resultant ZnO nanowire growth on UV exposed seed layers showed that the ZnO nanowires have good crystallinity. The XRD results, shown in figure 5, show the 2θ plot for the bare printed carbon on polyimide substrate (lower trace) and the as-grown ZnO nanowires on the printed carbon on polyimide substrate (upper trace). The spectra have been offset for clarity and show the characteristic ZnO peaks that are consistent with the hexagonal structure of ZnO. This confirms the nanowires are of wurtzite-type crystalline structure as demonstrated by the main ZnO peaks at 2θ = 34.31°, 31.67° and 36.14° assigned to the [100], [002] and [101] axes respectively. The dominance of the [002] peak shows a preferential growth direction along the c-axis and high quality of the resultant nanowires. The peak observed at 38.06° is an artefact of the carbon substrate and appears in both spectra, with and without ZnO nanowires.
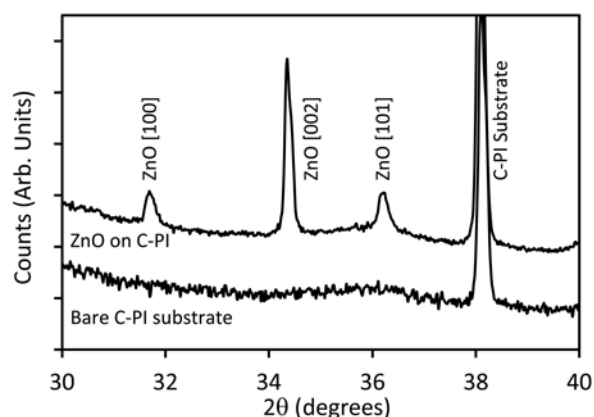

Figure 5: XRD analysis of the resultant ZnO nanowire growth on a seed layer after 25 seconds of UV exposure (upper trace) and bare printed carbon on polyimide substrate (lower trace).

It has been shown that the UV exposure technique provides a seed layer suitable for the growth of ZnO nanowires. The growth improves with increased UV exposure of the seed layer, up to 30 seconds, as shown in figure 3. However the growth appears to reduce in density with further increase

of exposure time beyond 30 seconds. This observed trend in the growth density is most likely due to the density of seeding crystals in the seed layer. A higher number of seeding sites will lead to a higher number of growth sites and therefore a higher density of ZnO nanowires.

It is expected that the nanowire diameter will be inversely proportional to the density of growth. This is due to the Zn^+ ion concentration of the growth solution at the surface of the growing nanowires. The growth reactions, and therefore consumption, of these Zn^+ ions during the growth process causes the Zn^+ ion concentration at the surface of the growing nanowires to decrease compared to the bulk concentration. This process gives rise to a concentration gradient within the growth solution towards the growing surface. The growth mechanism of ZnO nanowires proposed by Elias et al (Elias *et al* 2008) shows this in more detail. The magnitude of the concentration gradient at the surface is dependent on the rate at which the Zn^+ ions are consumed by the growing nanowires. Therefore more growth sites will result in a lower concentration of Zn^+ ions at the surface. Growths performed in solutions containing higher concentrations of zinc precursors tend to give rise to wires of increased diameter (Akgun *et al* 2012). Higher density growth, which results in a reduced surface concentration of Zn^+ ions from the growth solution, due to an increase in the number of growth sites, will therefore lead to ZnO nanowires of reduced diameter for the same growth parameters.

EDX analysis of UV exposed seed layers was performed to assess compositional changes in the zinc acetate layer with respect to UV exposure time. The structure of zinc acetate is $Zn(CH_3CO_2)_2$ therefore it is anticipated that a reduction of carbon and oxygen would be observed with an increase in UV exposure time. Zinc acetate has four oxygen and four carbon atoms. Since ZnO contains oxygen with a 1:1 stoichiometry to zinc and contains no carbon it is further anticipated that the reduction in carbon would be greater than the reduction in oxygen. The EDX analysis in figure 6 shows the oxygen to zinc and carbon to zinc ratios of the seed layer with respect to UV exposure time. EDX was carried out on seed layers deposited on to silicon substrates and is averaged over 6 spectra per sample. An acceleration potential of 5 kV was used and analysis was over the whole viewing area while imaging at 1k times magnification. The low acceleration potential of 5 kV reduces the penetration depth, as compared to higher acceleration potentials, while still allowing the 0.277 keV, 0.525 keV and 1.012 keV peaks to be observed which correspond to the carbon Kα, oxygen Kα and zinc Lα transitions respectively. Imaging over a larger area gives an averaging effect which gives more consistent results. The large area scan also reduces charging on the poorly conducting unexposed layers.

The EDX analysis shows that samples with no UV exposure have ratios of 3.3 and 2.7 for the oxygen to zinc and carbon to zinc respectively. These values are more consistent with basic zinc acetate which has the structure $Zn_4O(CH_3CO_2)_6$ giving expected oxygen to zinc and carbon to zinc ratios of 3.25 and 3 respectively. Basic zinc acetate is most likely being formed in the ink solution during the

solution phase. The trends in the atomic ratios shown in figure 6 confirm that the UV exposure is causing decomposition of the deposited layer. With increased UV exposure time, both the oxygen to zinc ratio and the carbon to zinc ratio decreases. A larger decrease in the carbon to zinc ratio than the oxygen to zinc ratio was observed. The decomposition shown in figure 6 would lead to a higher proportion of ZnO nanocrystallite seeds for samples undergoing more UV exposure and this explains the trend for up to 30 seconds of UV exposure shown in figure 3. With further increase in UV exposure, i.e. beyond 30 seconds, the EDX analysis shows little change. This indicates that the rate of decomposition of the zinc precursor reduces beyond 30 seconds of UV exposure and that the quantity of ZnO becomes constant. However, it is evident from the trends in the nanowire growth that the density of suitable seed crystals is decreasing. It is anticipated that only a fraction of the zinc precursor will undergo decomposition and mostly at the surface where the intensity of UV is greatest. The penetration depth for the EDX will be close to or beyond the thickness of the layer hence the ratios for the oxygen to zinc and carbon to zinc are not showing a change to 1 and zero respectively which would be expected for full conversion.
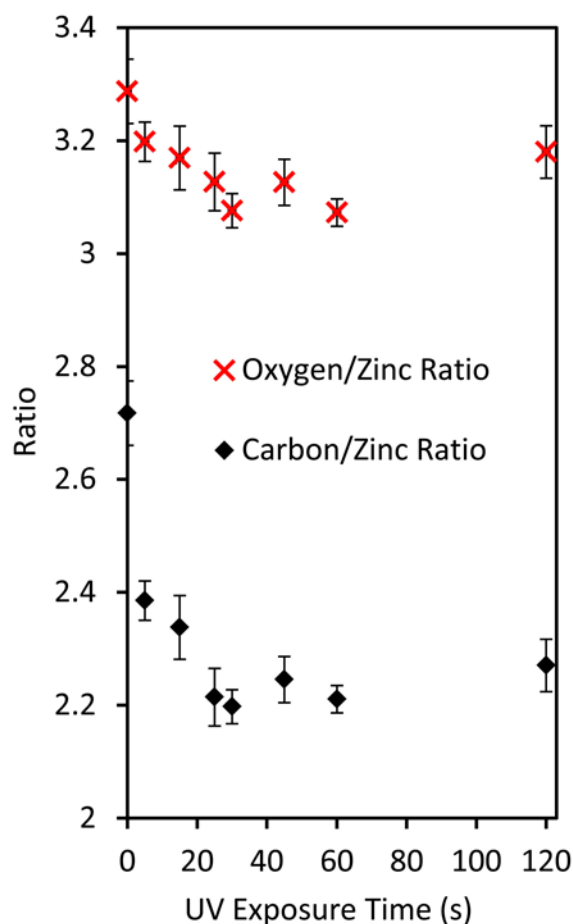

Figure 6: EDX compositional analysis of UV exposed zinc precursor layers showing the oxygen to zinc ratio (upper trace) and the carbon to zinc ratio (lower trace).

XPS analysis of the seed layers further confirms conversion of the zinc precursor to ZnO with exposure to UV. Detailed analysis of the Zn 2p peak was carried out. Figure 7(a) shows analysis for samples which have undergone no annealing. A fit to the obtained data is achieved with only one component at 1022.8 ± 0.1 eV, which corresponds to Zn-O-C=O, a structure consistent with zinc acetate or basic zinc acetate. For samples exposed to UV for 30 seconds a strong shift of the peak was observed and a good fit was given by two components at 1022.8 eV and 1021.8 eV which correspond to Zn-O-C=O and Zn-O respectively, further confirming the formation of ZnO in the layer. Compositional analysis revealed that after 30 seconds of exposure 72% of the signal was associated with Zn-O and 18% with Zn-O-C=O indicating strong conversion at the surface. The same analysis was carried out for a sample after 120 seconds of UV exposure which showed a similar conversion percentage. This indicates that more than 30 seconds of exposure has little effect on the composition of the seed layer. Figure 7(c) shows XPS data for a sample which was oven annealed for 30 minutes at 150°C which shows a fit with only one component at 1021.8 eV which corresponds to full conversion to ZnO.
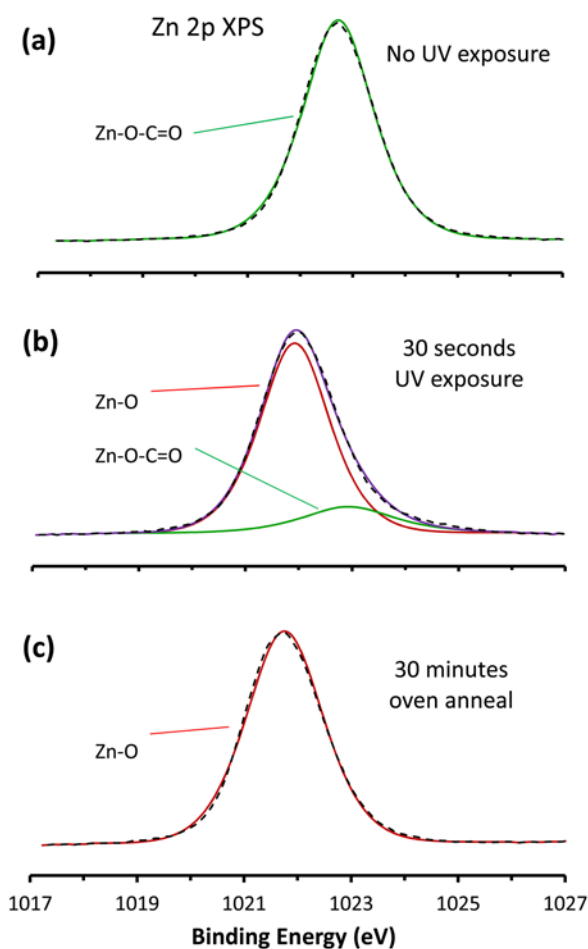

Figure 7: XPS analysis showing the Zn 2p peak (raw data is dashed line) of (a) seed layer with no UV exposure, (b) seed layer exposed for 30 seconds and (c) a seed layer after 30 minute oven annealing.

The trend shown in figure 3 suggests that the nucleation site density is at a maximum after 25 to 30 seconds of UV exposure. With less exposure time it is expected that insufficient decomposition of the zinc precursor has occurred. The reduction in nucleation site density for exposure times greater than 30 seconds could be attributed to surface morphology, for example grain size and surface roughness. This could be due to sintering of the ZnO layer reducing the density of nanocrystallites without reducing the quantity of ZnO. This is a low temperature method where the ambient temperature during the exposure did not rise above 46°C. However, the high UV flux and UV absorption properties of the zinc precursor and ZnO could induce localized heating within the thin layer making sintering possible without the need for the whole thickness of the substrate reaching sintering temperatures. Further evidence of this can be found in AFM images and Fourier image analyses. Figure 8(a-c) shows AFM images of seed layers exposed to no UV, 30 and 120 seconds of UV respectively. These images were levelled and filtered to remove low frequency curvature and high frequency noise while maintaining the surface features of the sample. The images clearly show that the surface texture and grain size is changing with UV exposure time. The images were also analysed using an average, line by line, Fourier transform which is shown in figure 9 for seed layers exposed to no UV, 30 and 120 seconds of UV respectively. The Fourier analyses highlights the change in surface morphology of the seed layers. This is shown by the increase in amplitude of lower frequency components with increased exposure time. This indicates that the features are growing in size with increased UV exposure and confirms the observations made subjectively from the images in figure 8. The analyses shows three peaks for a seed layer exposed for 30 seconds at frequencies that correspond to component wavelengths of 333nm, 200nm and 125nm from low to high frequency respectively. For the seed layer exposed for 120 seconds the dominant peak corresponds to long wavelengths of around 333nm which are much larger than many of the features in the seed layer exposed for just 30 seconds.
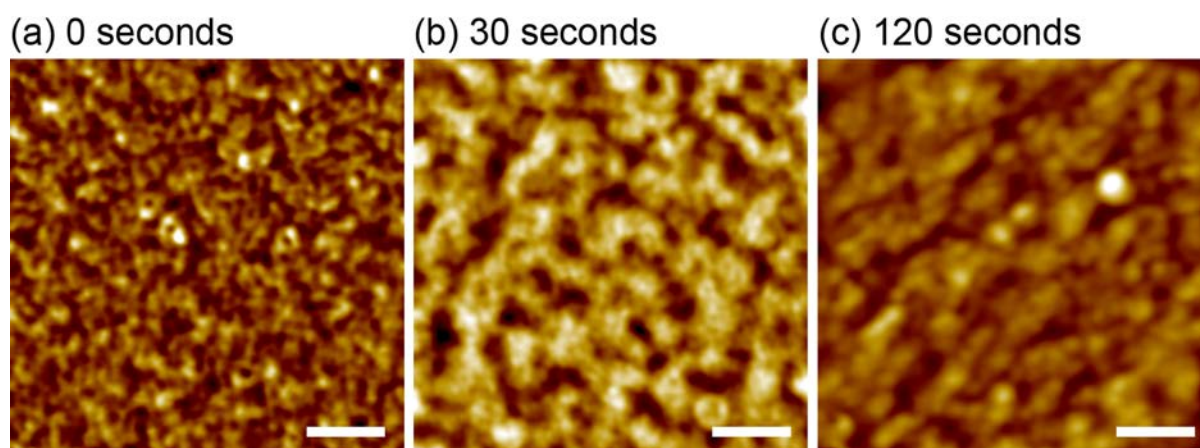

Figure 8: AFM images of seed layers after (a) no UV exposure, (b) 30 seconds of exposure and (c) 120 seconds of exposure with z-range of 1.24nm, 2.75nm and 6.21nm respectively. The scan size is 1μm x 1μm and the scale bars indicate 200nm.

With no UV exposure there are many small grains, which the EDX and XPS analyses indicate are not ZnO. Therefore this layer does not provide suitable seeding for the nucleation of ZnO nanowires. However, after 30 seconds of UV exposure larger particles were formed and from the EDX and XPS analyses these crystals, at the surface, are ZnO and form the nucleation sites required for the high quality growth shown in figure 2 and figure 3. Although the EDX and XPS show little change in the ratios beyond 30 seconds, the density of growth diminishes dramatically. Figure 8 (c) shows larger particles with increasing sample roughness for seed layers undergoing 120 seconds of UV exposure. Such change in morphology may be due to sintering of the ZnO nanocrystals at longer UV exposure time and could explain the decrease in the nanowire growth density as a result of diminished grain and grain boundary densities, which promote the nucleation of the ZnO nanowires.
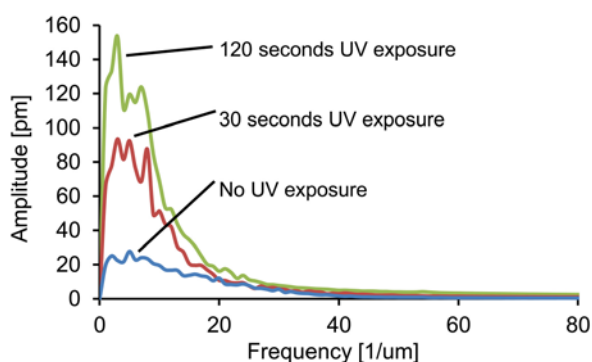

Figure 9: Fourier analysis for AFM images of seed layers after no UV exposure, 30 and 120 seconds of exposure.

4. Conclusion

This work has demonstrated the use of UV photodecomposition of zinc acetate to form suitable seed layers for the growth of ZnO nanowires. This technique significantly reduces the time and sample temperature required to create a suitable seed layer, reducing production time and allowing the use of low cost plastic substrates. The decomposition of the zinc acetate was confirmed with EDX and XRD analyses. Morphological changes were studied using AFM and showed an increase in topographical feature height with increased UV exposure. Fourier analysis showed increased amplitudes of low frequency components further indicated increased size of surface features. It was shown that the resultant ZnO nanowire growth performed on UV exposed seed layers was dependent on the UV exposure time. At the optimal exposure time of 25 to 30 seconds a maximum density of growth was achieved with a corresponding minimum in the nanowire diameters. This UV exposure technique could be coupled with the printing of zinc acetate inks previously reported by the authors using a roll to roll printing process such as flexographic printing. Production of devices, such as chemical and biological sensors, based on this technique is scalable and would bring the commercial use of such nanostructures significantly closer to realization.

5. Acknowledgement

6. References

Ahn J, Park H, Mastro M a, Hite J K, Eddy C R and Kim J 2011 Nanostructured n-ZnO / thin film p-silicon heterojunction light-emitting diodes. *Opt. Express* **19** 26006–10 Online: http://www.ncbi.nlm.nih.gov/pubmed/22274189

Akgun M C, Kalay Y E and Unalan H E 2012 Hydrothermal zinc oxide nanowire growth using zinc acetate dihydrate salt *J. Mater. Res.* **27** 1445–51 Online: http://www.journals.cambridge.org/abstract_S0884291412000921

Ali S M U, Ibupoto Z H, Salman S, Nur O, Willander M and Danielsson B 2011 Selective determination of urea using urease immobilized on ZnO nanowires *Sens. Actuators, B* **160** 637–43 Online: http://linkinghub.elsevier.com/retrieve/pii/S0925400511007647

Bai S-N 2011 Growth and properties of ZnO nanowires synthesized by a simple hydrothermal method *J. Mater. Sci. Mater. Electron.* **23** 398–402 Online: http://link.springer.com/10.1007/s10854-011-0440-8

Baruah S and Dutta J 2009a Effect of seeded substrates on hydrothermally grown ZnO nanorods *J. Sol-Gel Sci. Technol.* **50** 456–64 Online: http://link.springer.com/10.1007/s10971-009-1917-2

Baruah S and Dutta J 2009b Hydrothermal growth of ZnO nanostructures *Sci. Technol. Adv. Mater.* **10** 013001–19

Elias J, Tena-Zaera R and Lévy-Clément C 2008 Electrochemical deposition of ZnO nanowire arrays with tailored dimensions *J. Electroanal. Chem.* **621** 171–7 Online: http://linkinghub.elsevier.com/retrieve/pii/S0022072807004160

Fan H J, Werner P and Zacharias M 2006 Semiconductor nanowires: from self-organization to patterned growth. *Small* **2** 700–17 Online: http://www.ncbi.nlm.nih.gov/pubmed/17193109

Gowthaman P, Saroja M, Venkatachalam M, Deenathayalan J and Senthil T S 2011 Photocatalytic degradation of methelene blue dye using hydrothermally synthesized ZnO nanorods **5** 1307–11

Greene L E, Law M, Goldberger J, Kim F, Johnson J C, Zhang Y, Saykally R J and Yang P 2003 Low-temperature wafer-scale production of ZnO nanowire arrays. *Angew. Chem. Int. Ed. Engl.* **42** 3031–4 Online: http://www.ncbi.nlm.nih.gov/pubmed/12851963

Greene L E, Law M, Tan D H, Montano M, Goldberger J, Somorjai G and Yang P 2005 General route to vertical ZnO nanowire arrays using textured ZnO seeds. *Nano lett.* **5** 1231–6 Online: http://www.ncbi.nlm.nih.gov/pubmed/16178216

Guerguerian G, Elhordoy F, Pereyra C J, Marotti R E, Martín F, Leinen D, Ramos-Barrado J R and Dalchiele E a 2011 ZnO nanorod/CdS nanocrystal core/shell-type heterostructures for solar cell applications. *Nanotechnology* **22** 505401–10 Online: http://www.ncbi.nlm.nih.gov/pubmed/22108174

Hong S, Yeo J, Manorotkul W, Kang H W, Lee J, Han S, Rho Y, Suh Y D, Sung H J and Ko S H 2013 Digital selective growth of a ZnO nanowire array by large scale laser decomposition of zinc acetate. *Nanoscale* **5** 3698–703 Online: http://www.ncbi.nlm.nih.gov/pubmed/23494004

Hosono E, Fujihara S, Kimura T and Imai H 2004 Growth of layered basic zinc acetate in methanolic solutions and its pyrolytic transformation into porous zinc oxide films. *J. Colloid Interface Sci.* **272** 391–8 Online: http://www.ncbi.nlm.nih.gov/pubmed/15028503

Hsueh T-J, Lin S-Y, Weng W-Y, Hsu C-L, Tsai T-Y, Dai B-T and Shieh J-M 2012 Crystalline-Si photovoltaic devices with ZnO nanowires *Sol. Energy Mater. Sol. Cells* **98** 494–8 Online: http://linkinghub.elsevier.com/retrieve/pii/S092702481100643X

Huang M H, Mao S, Feick H, Yan H, Wu Y, Kind H, Weber E, Russo R and Yang P 2001 Room-temperature ultraviolet nanowire nanolasers. *Science (80-.).* **292** 1897–9 Online: http://www.ncbi.nlm.nih.gov/pubmed/11397941

Kar S, Pal B N, Chaudhuri S and Chakravorty D 2006 One-dimensional ZnO nanostructure arrays: synthesis and characterization. *J. Phys. Chem. B* **110** 4605–11 Online: http://www.ncbi.nlm.nih.gov/pubmed/16526691

Kitsomboonloha R, Baruah S, Myint M T Z, Subramanian V and Dutta J 2009 Selective growth of zinc oxide nanorods on inkjet printed seed patterns *J. Cryst. Growth* **311** 2352–8 Online: http://linkinghub.elsevier.com/retrieve/pii/S0022024809002620

Kwon J, Hong S, Lee H, Yeo J, Lee S S and Ko S H 2013 Direct selective growth of ZnO nanowire arrays from inkjet-printed zinc acetate precursor on a heated substrate. *Nanoscale Res. Lett.* **8** 489 Online: http://www.pubmedcentral.nih.gov/articlerender.fcgi?artid=3842827&tool=pmcentrez&rendertype=abstract

Liang Y N, Lok B K and Hu X 2009 Spatially selective patterning of zinc oxide precursor solution by inkjet printing *Proc. Electron. Packag. Technol. Conf., 11th* 174–9 Online: http://ieeexplore.ieee.org/lpdocs/epic03/wrapper.htm?arnumber=5416554

Liang Y N, Lok B K, Wang L, Feng C, Lu A C W, Mei T and Hu X 2013 Effects of the morphology of inkjet printed zinc oxide (ZnO) on thin film transistor performance and seeded ZnO nanorod growth *Thin Solid Films* **544** 509–14 Online: http://linkinghub.elsevier.com/retrieve/pii/S004060901300151X

Lim S K, Hwang S-H, Kim S and Park H 2011 Preparation of ZnO nanorods by microemulsion synthesis and their application as a CO gas sensor *Sens. Actuators, B* **160** 94–8 Online: http://linkinghub.elsevier.com/retrieve/pii/S0925400511006605

Lloyd J S, Fung C M, Deganello D, Wang R J, Maffeis T G G, Lau S P and Teng K S 2013 Flexographic printing-assisted fabrication of ZnO nanowire devices. *Nanotechnology* **24** 195602 Online: http://www.ncbi.nlm.nih.gov/pubmed/23579099

Ok J G, Tawfick S H, Juggernauth K A, Sun K, Zhang Y and Hart A J 2010 Electrically Addressable Hybrid Architectures of Zinc Oxide Nanowires Grown on Aligned Carbon Nanotubes *Adv. Funct. Mater.* **20** 2470–80 Online: http://doi.wiley.com/10.1002/adfm.201000249

Plakhova T V., Shestakov M V. and Baranov A N 2012 Effect of textured seeds on the morphology and optical properties of solution- and vapor-grown ZnO nanorod arrays *Inorg. Mater.* **48** 469–75 Online: http://www.springerlink.com/index/10.1134/S0020168512050135

Smith N a., Evans J E, Jones D R, Lord A M and Wilks S P 2015 Growth of ZnO nanowire arrays directly onto Si via substrate topographical adjustments using both wet chemical and dry etching methods *Mater. Sci. Eng. B* **193** 41–8 Online: http://linkinghub.elsevier.com/retrieve/pii/S0921510714002487

Song J and Lim S 2007 Effect of Seed Layer on the Growth of ZnO Nanorods *J. Phys. Chem. C* **111** 596–600 Online: http://pubs.acs.org/doi/abs/10.1021/jp0655017

Tarat A, Majithia R, Brown R A, Penny M W, Meissner K E and Maffeis T G G 2012 Synthesis of nanocrystalline ZnO nanobelts via pyrolytic decomposition of zinc acetate nanobelts and their gas sensing behavior *Surf. Sci.* **606** 715–21 Online: http://linkinghub.elsevier.com/retrieve/pii/S0039602811004791

Wahid K A, Lee W Y, Lee H W, Teh A S, Bien D C S and Azid I A 2013 Effect of seed annealing temperature and growth duration on hydrothermal ZnO nanorod structures and their electrical characteristics *Appl. Surf. Sci.* **283** 629–35 Online: http://linkinghub.elsevier.com/retrieve/pii/S0169433213012890

Wang L, Kang Y, Liu X, Zhang S, Huang W and Wang S 2012 ZnO nanorod gas sensor for ethanol detection *Sens. Actuators, B* **98** 237–43 Online: http://linkinghub.elsevier.com/retrieve/pii/S0925400511011634

Wang Z L 2004 Zinc oxide nanostructures: growth, properties and applications *J. Phys. Condens. Matter* **16** R829–58 Online: http://stacks.iop.org/0953-8984/16/i=25/a=R01?key=crossref.79a64bb3c5533760ca9ff098c9a46a8a

Yang K, She G-W, Wang H, Ou X-M, Zhang X-H, Lee C-S and Lee S-T 2009 ZnO Nanotube Arrays as Biosensors for Glucose *J. Phys. Chem. C* **113** 20169–72 Online: http://pubs.acs.org/doi/abs/10.1021/jp901894j

Yang T, Cheng K, Cheng G, Hu B, Wang S and Du Z 2014 Position-Controlled Hydrothermal Growth of Periodic Individual ZnO Nanorod Arrays on Indium Tin Oxide

Substrate *J. Phys. Chem. C* **118** 20613–9 Online:
http://pubs.acs.org/doi/abs/10.1021/jp505154p

Yi F, Liao Q, Yan X, Bai Z, Wang Z, Chen X, Zhang Q, Huang Y and Zhang Y 2014 Simple
fabrication of a ZnO nanorod array UV detector with a high performance *Phys. E Low-
dimensional Syst. Nanostructures* **61** 180–4 Online:
http://linkinghub.elsevier.com/retrieve/pii/S138694771400112X

Yoon H, Seo K, Moon H, Varadwaj K S K, In J and Kim B 2008 Aluminum Foil Mediated
Noncatalytic Growth of ZnO Nanowire Arrays on an Indium Tin Oxide Substrate *J.
Phys. Chem. C* **112** 9181–5 Online: http://pubs.acs.org/cgi-
bin/doilookup/?10.1021/jp800515y

Zacharias M, Subannajui K, Menzel A and Yang Y 2010 ZnO nanowire arrays - Pattern
generation, growth and applications *Phys. Status Solidi B* **247** 2305–14 Online:
http://doi.wiley.com/10.1002/pssb.201046399